Elimination of Boundary Effects at the Numerical Implementation of Continuous Wavelet Transform to Nonstationary Biomedical Signals

S. V. Bozhokin, I. B. Suslova and D. A. Tarakanov
Peter the Great Saint-Petersburg Polytechnic University, Polytechnicheskaya 29, Saint-Petersburg, Russia

Keywords: Continuous Wavelet Transform, Boundary Effects, Nonstationary Heart Tachogram.

Abstract: The main objective of the paper is to develop an algorithm improving the situation with boundary effects at the numerical implementation of continuous wavelet transform, what makes it possible to hold down important information in the study of many nonstationary biological signals. As a basis for the research, we propose the mathematical model of nonstationary signal (*NS)* with a complex amplitude variation in time. Such signals show peaks near the beginning and end of the observation period. The model leads to the analytical expression for continuous wavelet transform (*CWT*). Thus, we get to know how boundary effects relate to the finiteness in time of the mother wavelet function. To avoid boundary effects arising at the procedure of numerical wavelet transform, we develop the algorithm of signal time shift (*STS*). The results of analytical solution and numerical *CWT* calculation with and without the use of *STS* show the benefit of using *STS* in the processing of nonstationary signals. We have applied the technique to the study of nonstationary heart tachogram and discovered heart activity bursts in different spectral ranges, which appear and disappear at different time moments.

1 INTRODUCTION

The technique of *CWT* (continuous wavelet transform) allows us to develop a system of quantitative parameters for analysing nonstationary (*NS*) signals, with statistical and spectral properties changing in time (Mallat, 2008), (Cohen, 2003), (Advances in Wavelet, 2012), (Chui and Jiang, 2013), (Addison, 2017), (Hramov, 2015). The first important operation in the wavelet theory is the scaling procedure, in which we change the region of wavelet function localization in frequency. The second step is the shift operation, in which we change the localization of wavelet function in time. In this way, we can clearly reveal the amplitude-frequency properties of the signals under study. *CWT* represents three-dimensional surface $V(\nu,t)$ depending on frequency ν and time t. Analytical *CWT* calculations using the Morlet mother wavelet function show that for harmonic signal $Z(t)=\cos(2\pi f_0 t)$ (f_0 is the frequency), the maximum of $|V(\nu,t)|$ is reached at $\nu=f_0$, and this maximal value does not depend on t. In the case of two infinite harmonic signals with frequencies f_1, f_2 and the same amplitude, we observe the peaks of ridges with the same amplitude $|V(\nu,t)|$ at points $\nu=f_1$ and $\nu=f_2$ (Bozhokin, 2012), (Andreev et al., 2014), (Bozhokin and Suslova, 2013), (Bozhokin and Suslova, 2015), (Bozhokin et al., 2017). The majority of *CWT* studies use numerical calculations. In this case, the question arises of how accurately *CWT* reproduces the properties of $Z(t)$ given in the finite interval $t=[0,T]$ (T is the time of observation). The shortcoming of *CWT* is the finite temporal resolution of the mother wavelet function. This causes boundary effects near the initial and final moments of time, where we can observe significant differences in the amplitude-frequency properties of the original signal $Z(t)$ and its *CWT* image $V(\nu,t)$. To correct this drawback and improve the resolution of low frequency signal components in the case of short signal duration, the authors of (Tankanag and Chemeris, 2009), (Podtaev et.al.,2008), (Boltezar and Slavic, 2004), (Ulker-Kaustell and Karoumi, 2011) undertook a modification of *CWT* algorithm. The work (Cazelles et al.,2008) presents the discussion of boundary effects depending on the type of the mother wavelet function. The numerical estimation of

Bozhokin, S., Suslova, I. and Tarakanov, D.
Elimination of Boundary Effects at the Numerical Implementation of Continuous Wavelet Transform to Nonstationary Biomedical Signals.
DOI: 10.5220/0007254900210032
In *Proceedings of the 12th International Joint Conference on Biomedical Engineering Systems and Technologies (BIOSTEC 2019)*, pages 21-32
ISBN: 978-989-758-353-7

boundary effects at *CWT* for real experimental nonstationary signals was carried out in (Tankanag and Chemeris, 2009), (Podtaev et.al.,2008), (Boltezar and Slavic, 2004), (Ulker-Kaustell and Karoumi, 2011).

When analysing non-stationary signals in medicine, the development of quantitative parameters to describe heart rate variability is of great importance. Heart rate variability (*HRV*) inferred from the analysis of a tachogram—a series of *RR* intervals between heart contractions—is known as an important index in cardio-vascular system assessment (*CVS*) (Addison, 2017), (Baevskii et al, 2002), (Anderson et al, 2018), (Bhavsar et al. 2018), (Hammad et al, 2018). However, the statistical parameters of *HRV* (*RRNN*, *SDNN*, *RMSSD*), the spectral characteristics of cardio intervals employing the Fourier transform (*ULF*, *VLF*, *LF*, *HF*), and the histogram methods given in the Standards can be used only in stationary situations. The condition of stationarity, meaning the repetition of statistical and spectral characteristics of the cardio signal taken arbitrarily over any time segment, is not fulfilled in the majority of cardiac situations. In particular, it is true for the passive tilt test used for complex assessment of the cardiovascular system (*CVS*) to elucidate the mechanisms of its autonomous regulation. This test allows good standardization. The passive tilt test is performed on a special automated tilt table, which brings the body from the horizontal into the vertical position. There are two types of orthostatic tests, in which the human head rises (*HUT* –head up table) and in which the human head falls (*HDT* –head down table). Tilt tests are used to determine the tolerance of the organism to abrupt changes of body position in occupational selection (pilots and cosmonauts), prescription of drugs that affect blood redistribution in diagnosing neuro-circulatory disorders, and elucidation of the mechanisms of functional impairment of the autonomous system (*ANS*), in particular, detecting patients with neuro -cardiac fainting spells (syncope).

The wavelet theory has been successfully applied in *HRV* studies (Addison, 2017), (Keissar at al. 2009), (Ducla-Soares et al, 2007). Most *HRV* studies based on the wavelet theory use the models of amplitude-modulated signals, i.e., when the regular sampling interval Δt coincides with the mean *RR* interval (Δt = *RRNN*). However, in many actual situations, where it is necessary to analyze accurately the cardiac arrhythmia, the time points of heartbeats are spaced very irregularly. Thus, developing of new models to study the transitional processes in the heart rhythm, which occur very often, for example, at tilt tests, remains a pressing problem.

In the present paper, we develop an algorithm to eliminate boundary effects in the numerical implementation of the continuous wavelet transform. To solve this problem, we introduce the mathematical model of a signal with complextime variation in the amplitude $A(t)$. The model specifies the time behaviour of the amplitude, as well as the occurrence of peaks near the beginning and end of the observation period. This model allows us to obtain the analytical solution for the wavelet transform $V(\nu,t)$ and compare it with the given signal amplitude $A(t)$. To eliminate boundary effects arising at the numerical procedure of *CWT*, we propose the algorithm of signal time shift (*STS*).

The aim of the work is to use the developed method *STS* together with the technique of *CWT* for the quantitative description of non-stationary heart rate variability. In the model we propose here, the *HRV* signal is a superposition of the Gaussian peaks of the same amplitude. The centers of heart beats separated by RR_n time intervals are located on a substantially irregular grid, which is characterized by time points t_n, where $t_n = t_{n-1} + RR_n$, n = 1, 2, 3, …, N – 1, and $t_0 = RR_0$. These time points strictly correspond to the time points of the actual *RR* intervals. Our tachogram model considers frequency modulated signals and provides an analytical solution using *CWT* with the Morlet mother wavelet function. The maximal *CWT* value corresponds the value of local frequency function $F_{\max}(t)$ Applying the second *CWT (DCWT)* for the signal $F_{\max}(t)$ allows us to study both aperiodic and oscillory movements of the local frequency in *ULF*,*VLF*, *LF*, as well as the *HF* spectral ranges (Bozhokin and Suslova, 2013), (Bozhokin and Suslova, 2014), (Bozhokin et al, 2018).

2 METHODS

2.1 Mathematical Model of Nonstationary Signal

We consider nonstationary signal $Z(t)$ with the amplitude varying strongly in time. The characteristic feature of the proposed model is the complex behavior of the signal amplitude at time interval boundaries. We represent $Z(t)$ as a superposition of

N elementary nonstationary signals (*ENS)* centered in the points $t = t_L$ and determined by the system of *L* parameters:

$$Z(t) = \sum_{L=0}^{N-1} z_L\left(t - t_L\right). \quad (1)$$

ENS signal $z_L\left(t - t_L\right)$ in (1) has the shape of the Gaussian envelope of oscillating function (Bozhokin, 2012)

$$z_L\left(t - t_L\right) = \frac{b_L}{2\sqrt{\pi}\tau_L}\exp\left[-\frac{\left(t - t_L\right)^2}{4\tau_L^2}\right]\cos\left[2\pi f_L\left(t - t_L\right) + \alpha_L\right]. \quad (2)$$

Five parameters

$$L = (b_L; f_L; t_L; \tau_L; \alpha_L), \quad (3)$$

which determine the *ENS*, are: the amplitude b_L having the dimensions $(volt \times second)$; the frequency of oscillations f_L in *(Hz)*; the characteristic size τ_L of signal time localization in *(*s*);* the initial phase α_L in radians. Hereinafter, we assume that the condition $f_L\tau_L >> 1$ holds for all *ENS* considered in the present paper. This means that time interval τ_L, which equals the characteristic scale of amplitude decreasing, covers many oscillation periods $T_L = 1/f_L$.

As an example, we consider the signal $Z(t)$ (1) represented by four *ENS* (2) at L =0,1,2,3. Suppose the frequencies of all signals equal $f_L = 2\,Hz$, and their phases have zero values.

Table 1 displays all other parameters of the *ENS*. The parameters in Table 1 are chosen in such a way that the total signal has the form

$$Z(t) = B(t)\cos\left(2\pi f_0 t\right), \quad (4)$$

where f_0 =*2Hz*.

Table 1.

The parameters of four *ENS* in (1)			
L	b_L (s)	t_L (s)	τ_L (s)
0	–0.3	3	0.75
1	$10\sqrt{\pi}$	25	5
2	$-10\sqrt{\pi}$	25	4.5
3	–0.3	47	0.75

The value of $B(t)$ can be represented in the form

$$B(t) = \frac{1}{2\sqrt{\pi}}\sum_{L=0}^{N-1}\frac{b_L}{\tau_L}\exp\left[-\frac{\left(t - t_L\right)^2}{4\tau_L^2}\right]. \quad (5)$$

Let us introduce the notations

$$A(t) = \left|B(t)\right|,\ A(t)/A_m, \quad (6)$$

where A_m is the maximal value of the amplitude. Fig.1 shows the proposed model (1) of the signal. It is essential that the signal has the points of zero amplitude. Besides, the graph shows two high peaks with narrow localization τ_0 =0.75 *s* and τ_3 = 0.75 *s* at the beginning $t = 3\,s$, and at the end $t = 47$ *s* of the process.

Fig.2 shows the behavior of $A(t)/A_m$ within the interval $0 \le A(t)/A_m \le 1$.

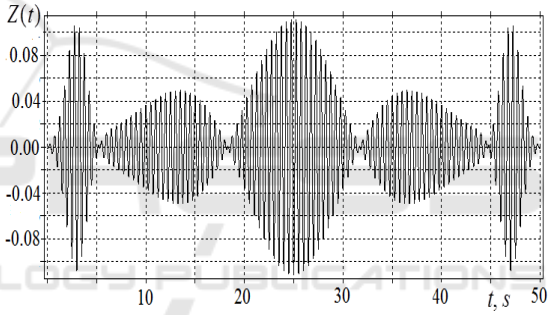

Figure 1: Time dependence of the signal $Z(t)$ (1) with the parameters given in Table 1.

It is important to emphasize that the proposed model allows us to set the amplitude exactly. Hereupon, the model gives the analytical solution for *CWT*.

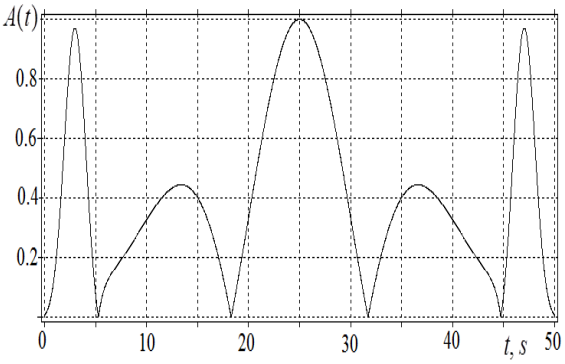

Figure 2: Dependence of $A(t)/A_m$ in time.

Further study will focus on computing *CWT*, formulating the criteria for determining how correctly *CWT* shows the time behavior of the amplitude $A(t)$, and eliminating boundary effects in *CWT* implementation.

2.2 Continuous Wavelet Transform

The continuous wavelet transform $V(\nu,t)$ (*CWT*) maps nonstationary signal $Z(t)$ with varying time-frequency structure on time-frequency plane (Addison, 2017), (Wavelet in Physics, 2004):

$$V(\nu,t)=\nu\int_{-\infty}^{\infty}Z(t')\psi^{*}\left(\nu(t-t')\right)dt', \tag{7}$$

where $\psi(x)$ is the mother wavelet function, and symbol * means complex conjugation. The mother wavelet $\psi(x)$ should be localized near the point $x=0$, have the unit norm value, and zero mean value calculated over the interval $-\infty<x<\infty$. The adaptive Morlet mother wavelet function (*AWM*), which we introduced in (Bozhokin et al. 2017), satisfies all these properties. The formulas for *AMW* and its Fourier image are

$$\psi(x)=D_m\exp\left(-\frac{x^2}{2m^2}\right)\left[\exp(2\pi ix)-\exp\left(-\Omega_m^2\right)\right], \tag{8}$$

$$\psi(F)=\frac{D_m\Omega_m}{\sqrt{\pi}}\exp\left[-\Omega_m^2(F-1)^2\right]\left[1-\exp\left(-2\Omega_m^2F\right)\right], \tag{9}$$

$$D_m=\frac{(2\pi)^{1/4}}{\sqrt{\Omega_m\left(1-2\exp\left(-\frac{3\Omega_m^2}{2}\right)+\exp\left(-2\Omega_m^2\right)\right)}}. \tag{10}$$

The value m in (8)-(10) plays the role of a control parameter, while $\Omega_m=m\pi\sqrt{2}$. The parameter of localization Δ_x, which indicates the extension of $\psi(x)$ along x-axis, and Δ_F, which corresponds to the extension of Fourier spectrum $\psi(F)$ (Mallat, 2018), (Chui and Jiang, 2013) along the frequency axis, have the values $\Delta_x\approx m/\sqrt{2}$, and $\Delta_F\approx 1/(\sqrt{8}\pi m)$. Their product is close to the lowest value $\Delta_x\Delta_F=1/(4\pi)$. The values of Δ_x and Δ_F vary with the change in m. Thus, we get the opportunity to vary the time and spectral resolution of the signals under study. At $m=1$ we obtain the formula for the ordinary Morlet mother wavelet function. If the characteristic length of $\psi(x)$ is $\Delta_x\approx m/\sqrt{2}$, the characteristic time moments, which make the main contribution to the integral (7), satisfy the relation

$$t-\frac{\Delta_x}{\nu}<t'<t+\frac{\Delta_x}{\nu}. \tag{11}$$

Thus, *AMW* (8) behaves like a varying window depending on the control parameter. The window width automatically becomes large for small frequencies and small for the large ones.

We note, that the wavelet transform (7) with the mother wavelet (8) for elementary nonstationary signals (2), with the amplitude varying in time and constant frequency, can be calculated analytically (Bozhokin et al, 2017). In this case, the maximum of $V_L(\nu,t)$ in frequency is achieved at the point, and the time behavior of $V_L(\nu,t)$ reproduces that of the signal amplitude. We can easily find the analytical expression of *CWT* for the superposition (1). The characteristic lengths $\Delta_t^{(\mathrm{CWT})}$ and $\Delta_\nu^{(\mathrm{CWT})}$ of $|V_L(\nu,t)|^2$ along the time and frequency axes have the values:

$$\Delta_t^{(\mathrm{CWT})}=\tau_L\sqrt{1+m^2/(2f_L^2\tau_L^2)}, \tag{12}$$

$$\Delta_\nu^{(\mathrm{CWT})}=\sqrt{1+2f_L^2\tau_L^2/m^2}/(4\pi\tau_L). \tag{13}$$

It is easy to derive two limiting cases of these formulas ($m\ll f_L\tau_L$ and $m\gg f_L\tau_L$).

2.3 Wavelet Analysis of Mathematical Model of Nonstationary Signal

After applying *CWT* with $m=1$ to (1), we can observe that at $\nu=f_L$ the time behavior $|V_L(f_L,t)|^2\approx\exp\left[-(t-t_L)^2/\left(2\tau_L^2\right)\right]$ exactly reproduces the time behavior of $A^2(t)$. If the control parameter $m\gg f_L\tau_L$, then the behavior of $|V_L(\nu,t=t_L)|^2$ exactly repeats the behavior of power spectrum $P(\nu)=|z_L(\nu)|^2$, and $\Delta_\nu^{(CWT)}$ exactly coincides with $\Delta_\nu^{(0)}$, which characterizes the width of *ENS* (2) power spectrum, i.e. $\Delta_\nu^{(\mathrm{CWT})}\approx\Delta_\nu^{(0)}=1/(4\pi\tau_L)$.

Fig.3 shows the complex amplitude and frequency properties of the signal.

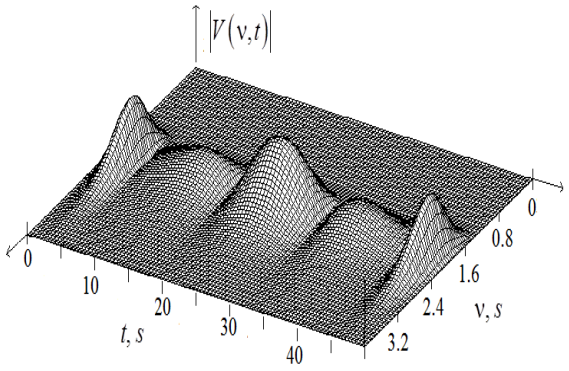

Figure 3: Analytical dependence of $|V(\nu,t)|$ on frequency $\nu(Hz)$ and time $t(s)$ for the signal $Z(t)$.

At t_L =3*s* (L =0) and t_L =47*s* (L =3) corresponding to the sharp peaks, we have wide frequency distribution. It is due to the fact that the length τ_L =0.75*s* of these peaks (L =0, L =3) is much smaller than the lengths of two other peaks τ_L =5*s* (L =1) and τ_L =4.5*s* (L =2). To find out how $|V(\nu,t)|$ reproduces the behavior of the signal amplitude $A(t)$, we make a cross-section of the surface at $\nu = f_0$ along the time axis. Fig.4 shows the cross-section of $|V(f_0,t)|$ in comparison with $A(t)$.

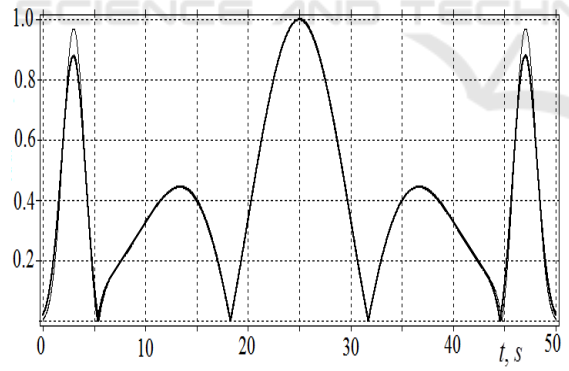

Figure 4: Comparison of time behavior for $A(t)$ (thin line) and cross section of $|V(f_0,t)|$ (bold line) at $m=1$.

In Fig. 4 we can see that the curves diverge only in a close neighborhood of peaks t_L =3*s* (L =0) and t_L =47*s* (L =3). It is because these two peaks are located at the beginning and at the end of the interval $[0,T]$, where the condition $f_L\tau_L >> 1$ is violated (f_0 =*2Hz*; $\tau_0 = \tau_3$ =*0.75s*). The curves nearly coincide at all other points of the interval $[0,T]$, where T =50*s*. We conclude that for $f_L\tau_L >> 1$, the curves $A(t)$ and $|V(f_0,t)|$ are similar. To characterize the deviation of $|V(f_0,t)|$ from $A(t)$, we introduce the parameter of mean square deviation by the formula

$$\sigma_t^2 = \frac{1}{T}\int_0^T \left[\frac{A(t)}{A_m} - \frac{|V(f_0;t)|}{V_m}\right]^2 dt, \qquad (14)$$

where V_m is the maximal value of $|V(f_0,t)|$ within the interval $[0,T]$. Thus, *CWT* with $m=1$ is well suited to describe the time variation of amplitude $A(t)$ for some specific moments, in which $A(t)$ =0 (Fig.2).

3 RESULTS

3.1 Boundary Effects in the Analysis of Spectral Properties

The foregoing results are based on the analytical expressions for $|V(\nu,t)|$ and $A(t)$ for the proposed mathematical model of nonstationary signal. For real signals, we are to carry out numerical calculations to find $|V(\nu,t)|$. In this case, we face the problem of boundary effects. Let us determine the influence of boundary effects in calculating $|V(\nu,t)|$ (Bozhokin and Suslova, 2013). Boundary effects can appear at both the left $(0 < t < t_{off})$ and the right $(T - t_{off} < t < T)$ ends of the observation interval T. The value of t_{off} will be determined later. The reason is the finite value of wavelet's length Δ_x, which leads to significant errors in numerical *CWT* calculation. To eliminate the errors, we take the values of $V(\nu,t)$ in these intervals equal to zero. Naturally, we lose the valuable information on the time-frequency behavior of the signal within these intervals. How can you keep this information?

Let us formulate the problem of finding the minimal value $\nu_{\min}$ of frequency that will allow us to determine *CWT* correctly. Analyzing (11), we conclude that in the initial interval $[0,t_{off}]$, the

$$t_{off} = \frac{2\Delta_x}{\nu_{\min}}. \quad (15)$$

A similar formula can be obtained near the right-hand boundary $\left[T - t_{off}; T\right]$ of the signal. To determine $\nu_{\min}$ correctly, we need n $(n >> 1)$ periods of frequency oscillations with the duration of $1/\nu_{\min}$ that can be placed within the remaining time interval $[T - 2t_{off}]$. The observation interval T consists of two boundary sections with the lengths $4\Delta_x / \nu_{\min}$ and $n/\nu_{\min}$ (the interval to determine *CWT* correctly). Then we have

$$\nu_{\min} = \frac{n + 4\Delta_x}{T}. \quad (16)$$

Taking into account the boundary effects leads to the value of $\nu_{\min}$ approximately $n + 4\Delta_x$ times largerthan $f_{\min} = 1/T$ used in the Fourier analysis. After determining $\nu_{\min}$ (16), we can calculate the value of t_{off} (15).

To eliminate boundary effects, we propose an algorithm, which we call Signal Time Shift (*STS*). Knowing the value $\nu_{\min}$ (16), we can extend the interval of signal observation from T to T_1. The beginning of the interval T $(t = 0)$ is transferred into the point $t_{\min}$, and the initial interval $\left[0; t_{\min}\right]$, which enters a new time period T_1, should be filled with the initial constant values of the signal $Z(t = 0)$. We are to choose the value of $t_{\min}$ larger than the initial section, where we can observe the boundary effects, i.e. $t_{\min} = 2.5\Delta_x / \nu_{\min}$. This value is larger than t_{off} $(t_{\min} = 1.25 t_{off})$. We also fill the new finite interval $\left[T_1 - t_{\min}; T_1\right]$ with the constant values $Z(t = T)$ of the signal. The central interval $[t_{\min}; T_1 - t_{\min}]$ at $T_1 > T$ has the duration T. It exactly repeats all the values of the investigated signal. Thus, the values of $Z(t)$ are located in the central part of the new interval T_1 outside the boundary effect zone.

The primary interval T is shown in the upper part of Fig.5. This interval consists of two boundary sections (in black) with the duration $2t_{off} = 4\Delta_x / \nu_{\min}$ plus the section with the duration $n/\nu_{\min}$. The lower

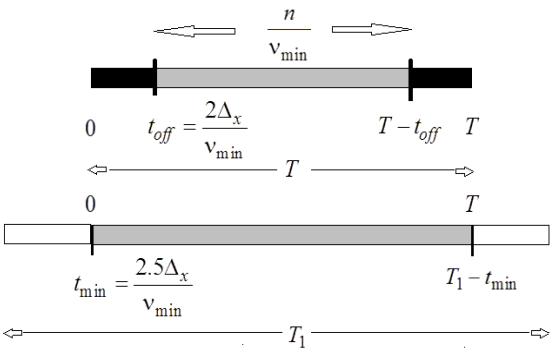

Figure 5: The upper drawing corresponds to the interval T with two boundary sections marked in black; the lower drawing corresponds to T_1.

drawing in Fig.5 shows the enlarged interval T_1, which consists of the central section T with all values of $Z(t)$ (in grey) and two sections of total duration $2t_{\min} = 5\Delta_x / \nu_{\min}$ with the boundary values of $Z(t)$. We make equal the minimum frequency values $\nu_{\min}(T) = \nu_{\min}(T_1)$ for T and $T_1 = T + 5\Delta_x / \nu_{\min}$. In this case, the number of periods $n(T)$ and $n_1(T_1)$ for correct determination of the frequency $\nu_{\min}$ are related to each other as $n_1(T_1) = n(T) + 5\Delta_x$. The next step in *STS* algorithm is numerical calculations of *CWT* in the interval $[0, T_1]$. Then, we eliminate all the values of $V(\nu, t)$ located at the beginning of $\left[0; t_{\min}\right]$ and at the end of $[t_{\min}; T_1 - t_{\min}]$. The subsequent shift of start timing from point $t = t_{\min}$ to the point t =0 restores the initial observation interval $t = \left[0; T\right]$, and allows us to compare the values of $V(\nu, t)$ with the true behavior of the signal $Z(t)$ taking into account the boundary effects.

Let us compare the analytical behavior of $A(t)$ (Fig.2) with that of $\left|V(f_0, t)\right|$ (*CWT*) (Fig.4), numerical implementation $\left|V^{(\text{num})}(f_0, t)\right|$ of *CWT* without the procedure of signal time shift (*STS*), and the numerical implementation $\left|V^{(sts)}(f_0, t)\right|$ of *CWT* with the use of *STS*. All calculations are carried out for the model (1)-(2) and the parameters given in Table 1. Numerical calculations are made for the Morlet wavelet with $m = 1$, the characteristic length Δ_x =1, the number of oscillation periods $n = 10$. In

this case, T =50s, $\nu_{\min}$ =0.28Hz, t_{off} =7.14s, $t_{\min}$ =8.93s, T_1 =61.76s.

Fig.6 represents a small fragment of the signal near the beginning to demonstrate the boundary effects. The duration is 5s. In Fig.6 the dash-dot line shows CWT calculated numerically $\left|V^{(\mathrm{num})}(f_0,t)\right|$, in which the boundary effects appear. For the frequencies $\nu \approx 1$ Hz, the cut-off time is $t_{off} \approx 2s$. We observe strong differences between $\left|V^{(\mathrm{num})}(f_0,t)\right|$ and $A(t)$ at times $0 < t < t_{off}$. This requires us to take as zeros the wrong values of $\left|V^{(\mathrm{num})}(f_0,t)\right|$ in the interval $0 < t < 2s$. The dot line represents the result $\left|V^{(sts)}(f_0,t)\right|$ of applying STS method. This line reproduces the analytical behavior of $\left|V(f_0,t)\right|$ quite well.

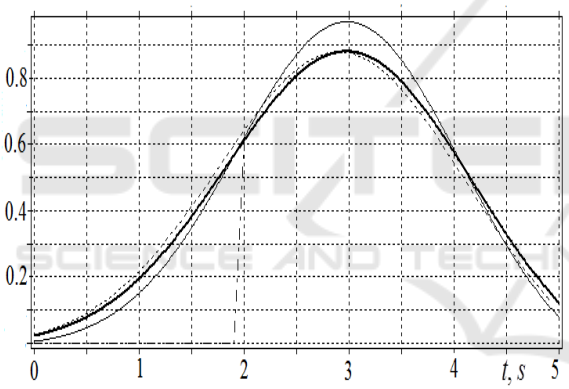

Figure 6: Thin line – $A(t)$; bold line – analytical $\left|V(f_0,t)\right|$; dash-dot line – numerical $\left|V^{(\mathrm{num})}(f_0,t)\right|$, which takes zero values at small times; dot line – numerical with the use of signal time shift.

Thus, the numerical implementation together with STS method allows us to save the important information about the amplitude–frequency behavior of the signal near the beginning and the end of the observation interval. The signal time shift allows us to consider all the time points of the signal under study.

3.2 *STS* Algorithm in the Analysis of Heart Tachogram

The method of eliminating boundary effects (*STS*), developed in the previous section, can be applied in the study of non-stationary signal representing the heart tachogram.

In contrast to the traditional approach of simulating the tachogram as an amplitude modulated signal with the points equidistant in time, we consider it as a frequency-modulated signal (Bozhokin and Suslova, 2013). We represent the heart tachogram signal as a set of identical Gaussian peaks, whose centers t_n are located on an uneven grid of times, and coincide in time with the true moments of heart beats: $t_n = t_{n-1} + RR_n$, n = 1, 2, 3, …, N – 1, and $t_0 = RR_0$. The width $\tau_0 = 20$ ms of each Gaussian peak is equal to the width of the *QRS* complex.

$$Z(t) = \frac{1}{2\tau_0\sqrt{\pi}} \sum_{n=0}^{N-1} \exp\left[-\frac{(t-t_n)^2}{4\tau_0^2}\right]. \qquad (17)$$

Such a model makes it possible to obtain the analytic expression for $V(\nu,t)$ (7). Fig.7 shows human heart tachogram registered during Head Down Tilt Test. It consists of three stages: A,B,C.

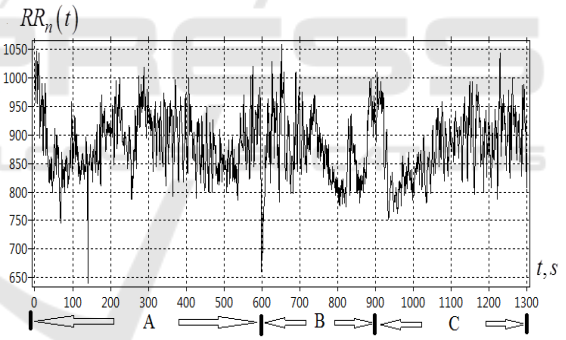

Figure 7: Dependence of heart bear interval RR_n on time $t(ms)$.

Stages A,C correspond to the horizontal position of the table. Stage B is the lowering of the table with a turn of 30°, which leads to the transients in the frequency of heart beats.

Let us consider the experimental tachogram (Fig.7) registered during head-down tilt test (*HDT*) The duration of intervals RR_n between the centers of heartbeats changes. Stage B, when the *HDT* takes place, lasts 300 s ($600 \le t \le 900$ s). For the proposed model of tachogram (17), the Gaussian peaks (17) are centered at the times t_n when heartbeats occur: $t_n = t_{n-1} + RR_n$, n = 1, 2, 3, .. N –1, and $t_0 = RR_0$.

Substituting these t_n into (17), we obtain the frequency-modulated tachogram signal $Z(t)$. The analytical expressions for the signal (17) and the mother wavelet function $\psi(x)$ (8) allow us to find the analytical expression for *CWT* (7). The value $F_{\max}(t)$ shown in Fig. 8 corresponds to the maximum value of $|V(\nu,t)|$ for each point in time t. The function $F_{\max}(t)$ varies in the range $0.4\,Hz \le F_{\max}(t) \le 2.5\,Hz$.

The study of $F_{\max}(t)$ during *HDT* (stage B, $600s \le t \le 900s$) shows the appearance of low-frequency oscillations. The characteristic period t_F of such oscillations approximately equals $100\,s$. In Fig.7 the graph for $RR_n(t)$ shows two heartbeats at the time $t \approx 600\,s$ separated by the interval $RR_n(t) \approx 650\,ms$. Therefore, at the same moment $t \approx 600\,s$, the value of $F_{\max}(t) \approx$ 1.54 *Hz* (Fig. 8). Thus, for the frequency-modulated signal (17) simulation, we can calculate the maximum local frequency $F_{\max}(t)$ at any time t.

Another wavelet transform applied to $F_{\max}(t)$ (double continuous wavelet transform *DCWT* [9]) makes it possible to study transients in the variation of frequency. Applying double continuous wavelet transform to the signal $F_{\max}(t)$ allows us to detect both aperiodic and oscillatory movements of the local frequency relative to the trend.

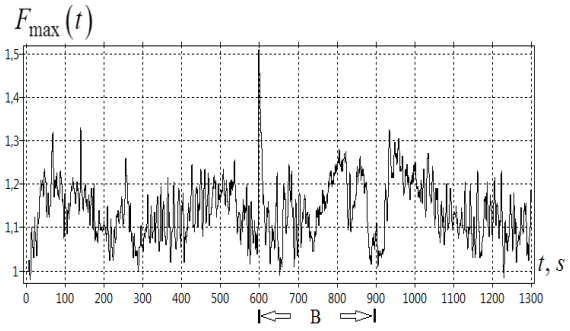

Figure 8: Dependence $F_{\max}(t)$ on time $t(ms)$.

Fig.9 displays the result of *DCWT* with the procedure of *STS*, which shows a sharp change in the spectral structure of the signal at stage B.

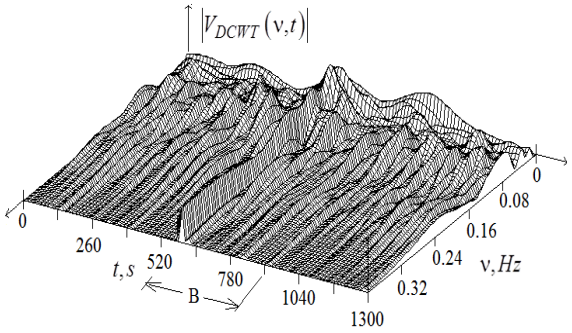

Figure 9: Dependence of double wavelet transform $|V_{DCWT}(t)|$ on frequency $\nu(Hz)$ and time $t(ms)$.

Fig. 9 shows that the tachogram is an alternation of bursts of spectral activity in different spectral ranges:
ULF = ($\nu_{\min}$;0.015 *Hz)*; (*VLF* = (0.015; 0.04 *Hz*); *LF* = (0.04; 0.15 *Hz*); *HF* =(0.15; 0.4 *Hz).*

The value of $\nu_{\min}$ is determined by the equation (16), with the number of periods $n = 5$, $\Delta_x = 2$.

To analyze heart tachogram during nonstationary functional tests, we introduced quantitative characteristics describing the dynamics of changes in spectral properties of the signal $F_{\max}(t)$. Such characteristics are the instantaneous spectral integrals $E_\mu(t)$, and the mean values of the spectral integrals $< E_\mu(S) >$ at the stages $S = \{A,B,C\}$ in different spectral ranges $\mu = \{ULF, VLF; LF; HF\}$.

To study the appearance and disappearance of low-frequency oscillations $F_{\max}(t)$, we can calculate the skeletons of *DCWT* showing the extreme line of $|V_{DCWT}(t)|$ on the plane ν and t. The value $\varepsilon(\nu,t)$ illustrates instantaneous frequency distribution of the signal energy (local density of energy spectrum of the signal)

$$\varepsilon(\nu,t) = \frac{2}{C_\Psi} \frac{|V_{DCWT}(\nu,t)|^2}{\nu} \qquad (18)$$

The constant C_Ψ for the Morlet mother wavelet (8) is approximately 1.013 ($m = 1$). The dynamics of time variation for different frequencies is determined by spectral integral $E_\mu(t)$:

$$E_\mu(t)=\frac{1}{\Delta\nu}\int_{\nu_\mu-\Delta\nu/2}^{\nu_\mu-\Delta\nu/2}\varepsilon(\nu,t)d\nu \qquad (19)$$

Spectral integral $E_\mu(t)$ represents the average value of the local density of the signal energy spectrum integrated over a certain frequency range $\mu=[\nu_\mu-\Delta\nu/2;\nu_\mu+\Delta\nu/2]$, where ν_μ denotes the middle of the interval, $\Delta\nu$ – its width. The time-variation of $E_\mu(t)$ performs a kind of signal filtration summing the contributions from the local density of the spectrum $\varepsilon(\nu,t)$ only in a certain range of frequencies μ={*ULF*, *VLF*, *LF*, *HF*}. By studying *D*CWT of the signal and calculating $E_\mu(t)$ in μ-range one can follow the dynamics of appearance and disappearance of low-frequency spectral components $F_{\max}(t)$.

The quantitative characteristics that describe the average dynamics of the spectral properties of a tachogram during nonstationary test have average values of the spectral integrals at the stages S={A,B,C} in the ranges μ. Assuming that stage S starts at $t_I(S)$ and ends at $t_F(S)$, the average spectral integrals are equal at stage S and are

$$<E_\mu(S)>=\frac{1}{\left[t_F(S)-t_I(S)\right]}\int_{t_I(S)}^{t_F(S)}E_\mu(t)dt. \qquad (20)$$

We introduce the function

$$d_\mu(t)=\frac{E_\mu(t)}{<E_\mu(A)>}, \qquad (21)$$

which shows the instantaneous value of the spectral integral in μ range at the arbitrary time point t as compared to its average value at rest (Stage A). In addition, we introduce the function $d_{\mu/\nu}(t)$:

$$d_{\mu/\nu}(t)=\frac{E_\mu(t)<E_\nu(A)>}{E_\nu(t)<E_\mu(A)>}, \qquad (22)$$

which shows how the instantaneous ratio $E_\mu(t)/E_\nu(t)$ varies over the ratio of average spectral integrals $<E_\mu(A)>/<E_\nu(A)>$ calculated at the stage of rest (Stage A). The functions $d_\mu(t)$ and $d_{\mu/\nu}(t)$ represent the variation of spectral characteristics during the total tachogram period as compared with the respective average values observed at Stage A (μ={*ULF, VLF, LF, HF*}; ν ={*ULF, VLF, LF, HF*})

We determine the heart rhythm assimilation coefficient in the spectral range μ as

$$D_\mu(B/A)=\frac{<E_\mu(B)>}{<E_\mu(A)>}. \qquad (23)$$

It reports the fold increase in the average spectral integral $<E_\mu(B)>$ for the μ-range at Stage B relative to the average value $<E_\mu(A)>$ of spectral integral for the same μ-range at rest (Stage A).

The detailed calculations of $E_\mu(t)$ and $<E_\mu(S)>$ are given in (Bozhokin and Suslova, 2013), (Bozhokin et al., 2017). Fig. 10-13 represent the results of *DCWT* analysis of nonstationary heart rhythm using the *STS* technique.

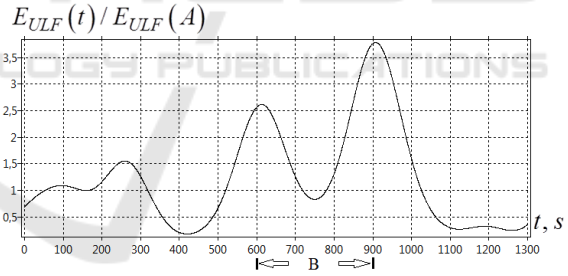

Figure 10: Spectral interval $E_{ULF}(t)$ divided by the average value in the stage A $E_{ULF}(A)$.

Fig.10 gives the plot of time behavior for $d_{ULF}(t)$ (21). The heart rhythm assimilation coefficient $D_{ULF}(B/A)$ (23) in the $\mu=ULF$ spectral range is 1.92. The coefficient $d_{ULF}(t)$ (21) reaches the maximal value ≈ 3.8 at $t\approx 900$ *s*. This means that the instantaneous value of $E_{ULF}(t)$ at Stage B (test phase) is approximately 3.8 times greater than the average value of $E_{ULF}(A)$ at Stage A (at rest). In this spectral range (*ULF*) during the

time period $600 \le t \le 900\ s$ a strong trend in $F_{\max}(t)$ is noticeable (Fig.8).

After the completion of *HDT* ($t > 900\ s$), there occurs a slow relaxation of the heart rate to the equilibrium state, which takes about 300 *s*. The characteristic time of frequency changes is equal to 100 *s*.

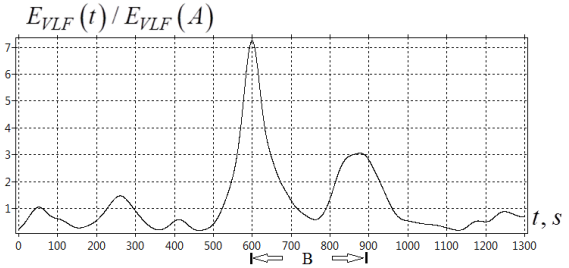

Figure 11: Spectral integral $E_{VLF}(t)$ divided by its average value $E_{VLF}(A)$ at the stage A.

Fig.11 shows the behavior of $d_{VLF}(t)$ (21). The heart rhythm assimilation coefficient $D_{VLF}(B/A)$ in the $\mu = VLF$ spectral range equals 2.32 (23). The maximum of $d_{ULF}(t) \approx 7.4$ (21) takes place at $t \approx 600\ s$. Fig.11 shows rapid *VLF* rhythm activation at Stage B ($600 \le t \le 900\ s$) in comparison to Stage A ($0 \le t \le 600\ s$).

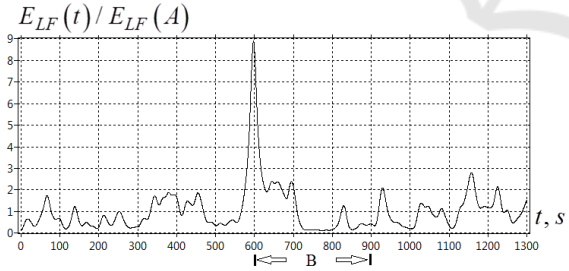

Figure 12: Spectral interval $E_{LF}(t)$ divided by its average value $E_{VLF}(A)$ at the stage A.

Fig.12 represents the coefficient $d_{LF}(t)$ as a function of time. Note that at Stage B in the range $\mu = LF$, the rhythm is also noticeably higher than at stage A. The heart rhythm assimilation coefficient $D_{LF}(B/A) = 1.15$. Considering the oscillatory motion of the maximal frequency $F_{\max}(t)$, we detect flashes of vibrational activity in this spectral range *LF* = (0.04; 0.15 *Hz*). For such flashes, the magnitudes of spectral integrals can many times exceed the background signal activity.

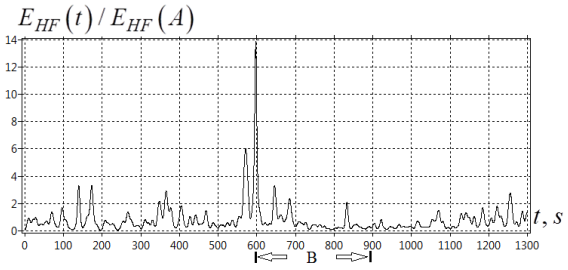

Figure 13: Spectral interval $E_{HF}(t)$ divided by its average value $E_{HF}(A)$ at the stage A .

In the range *HF* = (0.15; 0.4 *Hz*), we can also observe short flashes of activity in spectral integrals. The maximum of $d_{HF}(t)$ is approximately 14 times greater than the background, but $D_{HF}(B/A) = 0.67$. This means that the average activity at Stage B is less than the average activity at Stage A.

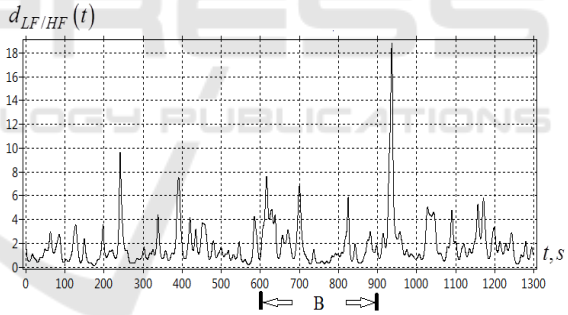

Figure 14: Temporal dependence of $d_{LF/HF}(t)$.

Fig.14 demonstrates the temporal behavior of $d_{LF/HF}(t)$, which characterizes the instantaneous ratio of $E_{LF}(t)/E_{HF}(t)$ to the average value $<E_{LF}(A)>/<E_{HF}(A)>$ calculated at stage A. The graph shows that at some time points the instantaneous value $d_{LF/HF}(t)$ becomes significantly large. This indicates the moments of tension in the physiological state of the patient and can be used for diagnostic purposes.

4 CONCLUSION

The algorithm developed in the article, which allows eliminating boundary effects in the numerical implementation of *CWT*, becomes especially important in the case of signals with the predominant influence of low frequencies, when the observation period for such signals is not too large. If the signal shows significant variations, the information on the behavior of the signal at the initial and final observation stages becomes very important for the correct conclusion about its amplitude-frequency properties.

We believe that as biological signals are strongly nonstationary, special technique is necessary to detect variations in frequency and temporal structure. Using *CWT* and *DCWT* with the *STS* procedure of boundary effect correction helps to solve the problem. The effectiveness of the technique is demonstrated in application to the record of human heart tachogram during functional test (*HDT* – head down).

The calculations were made based on the frequency-modulated tachogram model proposed by the authors. The technique of double continuous wavelet transformation leads to the conclusion that nonstationary tachogram can be represented as a combination of activity flashes in different spectral ranges. Such flashes may appear and disappear at certain points in time and in different spectral ranges. The quantitative characteristics of nonstationary tachogram estimate the increased heart activity in the period of changing the position of the body during the *HDT*.

The method of studying the restructuring spectral activity in the cardiac rhythm during the transitional processes, which is suggested in this article, makes it possible to reveal the dynamics of interaction between parasympathetic and sympathetic parts of the human autonomic nervous system. The proposed quantitative parameters allow us to get an objective assessment of the adaptive capabilities of the human organism during various physical, orthostatic, respiratory, psycho-emotional and medicated tests.

The proposed techniques help to reveal and analyze important information, which can be used in diagnostics.

ACKNOWLEDGMENTS

The work has been supported by the Russian Science Foundation (Grant of the RSF 17-12-01085).

REFERENCES

Addison, P.S. (2017) The illustrated wavelet transform handbook. Introductory theory and application in Science, engineering, medicine and finance. Second Edition, CPC Press.

Advances in Wavelet Theory and Their Applications in Engineering, Physics and Technology. (2012). Edited by Dumitru Baleanu.

Anderson, R., Jonsson, P., Sandsten, M. (2018). Effects of Age, BMI, Anxiety and Stress on the Parameters of a Stochastic Model for Heart Rate Variability Including Respiratory Information, *Proc. of the 11th International Joint Conference on Biomedical Engineering Systems and Technologies (BIOSTEC 2018), 4: BIOSIGNALS, P. 17-25.*

Andreev, D.A., Bozhokin, S.V., Venevtsev, I.D., Zhunusov, K.T. (2014). Gabor transform and continuous wavelet transform for model pulsed signals. *Technical Physics, 59(10):1428-1433.*

Baevskii, R.M., Ivanov, G.G., Chireikin, L.V., et. al., (2002). Analysis of heart rate variability using different cardiological systems: methodological recommendations. *Vestn. Aritmol., N.24: 65-91.*

Bhavsar, R., Daveya, N., Sun,Y., Helian, N., (2018). An Investigation of How Wavelet Transform Can Affect the Correlation Performance of Biomedical Signals. *Proc. of the 11th International Joint Conference on Biomedical Engineering Systems and Technologies (BIOSTEC 2018). V. 4: BIOSIGNALS, P. 139-146.*

Boltezar, M., Slavic, J., (2004). Enhancements to the continuous wavelet transform for damping identification on short signals. *Mechanical systems and signal processing, 18: 1065-1076.*

Bozhokin, S.V., (2012). Continuous Wavelet Transform and Exactly solvable Model of Nonstationary Signals. *Technical Physics, 57(7): 900-906.*

Bozhokin, S.V., Suslova, I.M., (2013). Double Wavelet Transform of Frequency-Modulated Nonstationary Signal. *Technical Physics, 58(12):1730-1736.*

Bozhokin, S.V. Suslova, I.B., (2014). Analysis of non-stationary HRV as a frequency modulated signal by double continuous wavelet transformation method. *Biomedical Signal Processing and Control. 10: 34-40.*

Bozhokin S.V., Suslova I.B., (2015). Wavelet-based analysis of spectral rearrangements of EEG patterns and of non-stationary correlations. *Physica A. 421: 151–160.*

Bozhokin, S.V., Zharko, S.V., Larionov, N.V., Litvinov, A.N., Sokolov, I.M. (2017). Wavelet Correlation of Nonstationary Signals. *Technical Physics, 62(6):837-845.*

Bozhokin, S.V., Lesova, E.M., Samoilov, V.O., Tarakanov D.E., (2018). Nonstationary heart rate variability in respiratory tests. *Human Physiology, 44(1):49-57.*

Cazelles, B, Chavex, M., Berteaux, D., Menard, F., Vik, J.O., Jenouvrier, S., Stenseth, N.C. (2008). Wavelet analysis of ecological time series. *Oecologia,156:297-304.*

Chui, C.K., Jiang O., (2013). *A*pplied Mathematics. Data Compression, Spectral Methods, Fourier Analysis, Wavelets and Applications. Mathematics Textbooks for Science and Engineering, v.2, Atlantis Press.

Cohen A., (2003). Numerical Analysis of Wavelet Method.,North-Holland, Elsevier Science.

Ducla-Soares, J.L., Santos-Bento, M., Laranjo, S.,et al., (2007).Wavelet analysis of autonomic outflow of normal subjects on head-up tilt, cold pressor test, Valsalva manoeuvre and deep breathing. *Exp. Physiol. 92(4): 677-686.*

Hammad, M., Maher, A., Adil, K., Jiang, F., Wang, K., (2018). Detection of Abnormal Heart Conditions from the Analysis of ECG Signals. *Proc. of the 11th International Joint Conference on Biomedical Engineering Systems and Technologies (BIOSTEC 2018). V. 4: BIOSIGNALS, P. 240-247.*

Hramov, A.E., Koronovskii, A.A., Makarov, V.A., Pavlov, A.N., Sitnikova, E., (2015). Wavelets in neuroscience, Springer Series in Synergetics, Springer-Verlag, Berlin, Heidelberg.

Keissar, K., Davrath, L.R., and Akselrod, S. (2009). Coherence analysis between respiration and heart rate variability using continuous wavelet transform. *Philos. Trans. R. Soc., A. 367(1892):1393-1406.*

Mallat, S., (2008). A Wavelet Tour of Signal Processing, 3rd ed., Academic Press, New York.

Podtaev S., Morozov M., Frick P., (2008). Wavelet-based corrections of skin temperature and blood flow oscillations. *Cardiovascular Engineering, 8(3):185-189.*

Tankanag, A.V., Chemeris, N.K., (2009). Adaptive wavelet analysis of oscillations in the Human peripherical blood flow. *Biophysics, 4(3):375-380.*

Ulker-Kaustell, M., Karoumi, R. (2011). Application of the continuous wavelet transform on the free vibration of a steel-concrete composite railway bridge. *Engineering structures, 33: 911-919.*

Wavelets in Physics, (2004). Edited by J.C. Van.den Berg, Cambridge University Press.